

ADVANCED MATERIALS

Supporting Information

for *Adv. Mater.*, DOI: 10.1002/adma.201905740

Built-In Active Microneedle Patch with Enhanced Autonomous Drug Delivery

*Miguel Angel Lopez-Ramirez, Fernando Soto, Chao Wang,
Ricardo Rueda, Sourabh Shukla, Cristian Silva-Lopez, Daniel
Kupor, David A. McBride, Jonathan K. Pokorski, Amir
Nourhani, Nicole F. Steinmetz,* Nisarg J. Shah,* and Joseph
Wang**

Supporting Information

Built-in Active Microneedle Patch with Enhanced Autonomous Drug Delivery

Miguel Angel Lopez-Ramirez, Fernando Soto, Chao Wang, Ricardo Rueda, Sourabh Shukla, Cristian Silva-Lopez, Daniel Kupor, David A. McBride, Jonathan K. Pokorski, Amir Nourhani, Nicole F. Steinmetz, Nisarg Shah* and Joseph Wang**

Supporting Information Figures

Figure s1. 3D height microscopy profile image of a 3x3 microneedle array.

Figure s2. Theoretical loading of a characteristic MN patch containing 225 conical MN tips

Figure s3. Active particle microneedle performance, activation and lifetime.

Figure s4. Schematic and time lapse images of the dissolution rate and fluid mixing of PVP microneedle under different experimental conditions.

Figure s5. Mean square displacement of tracer particles in presence of Mg particles at different pH.

Figure s6. Tuning the capabilities of Mg particles to control a delayed activation.

Figure s7. Microneedles loaded with smaller 20 μm Mg particles.

Figure s8. Amperometric curves of IgG-HRP from 3 release kinetics microneedle controls.

Figure s9. UV-vis spectrum of released Ab (IgG-AlexaFluor-555) from diffusion and active MNs at different time points.

Figure s10. Tumor volume growth curve of blank active microneedles.

Figure s11. Histological assessment of the kidney, liver, lung, and spleen in PBS-treated and active MN treated mice.

Figure s12. Stereolithography 3D printing and fabrication steps of polymeric combinatorial microneedle patch.

Supporting Information Videos

Video s1. Activity of Mg particles of different size in the presence of 10 μm PS tracer particles.

Video s2. Time frame microscopy images of the dissolution of passive vs active microneedles in the presence of tracer particles.

Video s3. Fluorescence video of the dissolution of active microneedles loaded with Rh6G.

Video s4. Top view FITC diffusion by passive vs active microneedles into phantom tissue.

Video s5. Animation of active microneedles into skin.

Experimental Section

PDMS microneedle mold fabrication: The master microneedle mold was placed in a clean Petri Dish, Crystal Clear Borosilicate Glass with a double-sided tape to attach the mold properly. A mix ratio of 10:2 base/curing agent PDMS (SYLGARD[®] 184, Sigma Aldrich) solution was later casted onto the microneedle patch and placed in vacuum within a desiccator for 5 min at 23 in of Hg. Bubbles were removed from the surface and PDMS was cured in an oven at 75C for 30 min. Later sample was removed from the oven and cured PDMS was separated from petri dish gently to obtain the negative mold. PDMS mold was adjusted to desired size with the use of a blade cut. The microneedle molds were washed with hand soap and rinsed with water twice, with further ultrasonication bath for 15 min. Later, the mold was dried with air gun and cleaned by adding 0.25 mL of 2-propanol to each mold for 10 min. Molds were placed in the oven (75C for 15 min) and not used until they reached room temperature.

Microneedle Patch Fabrication: A volume of 0.25 mL of a 10% w/v polymer (Polyvinylpyrrolidone (PVP) average $M_w \sim 360,000$, Sigma Aldrich) aqueous solution of pH 10.5 was added onto the PDMS MN mold and further placed in a closed desiccator in vacuum for 5-10 min (23 in Hg). Molds were removed from desiccator with the further removal of

bubbles generated at interface between MN pores and solution with the use of plastic 1mL disposable transfer pipettes or the use of a tweezer. Later, bubbles in the surface of the solution were removed, or popped with the use of a pipette or needle tip. Furthermore, a second addition of 0.25 mL of polymer was carried out, turning on vacuum again. This process was performed until polymer solution was 1 mL. The payload solution: 50 μ g of IgG-HRP(HRP-Goat anti-human IgG Antibody peroxidase from Vector Laboratories), 50 μ g of IgG-AlexaFluor555 (Abcam), 20 μ g of Rh6G (Sigma Aldrich), 20 μ g of FITC(Sigma Aldrich), or 100 μ g of anti-CTLA-4 (100 μ g, Clone, 9H10, BioXcell) was added to the mold and let it to dry for 24-72 hours. Once microneedle patches were ready, a 1 cm² scotch tape was applied on top of the needles and peeled off from the PDMS mold. Microneedle patches were stored at room temperature prior to use. Active microneedles were fabricated by employing the same procedure but before casting the polymer onto the mold, 50 μ L of a 5mg/mL stock Mg microparticle (catalog #FMW40, from TangShanWeiHao Magnesium Powder Co., Ltd China) in isopropanol suspension was casted and infiltrated within the negative MN features of the PDMS mold. A PVP solution of pH 10.5 was used to prevent Mg particles to react, ensuring a proper microneedle patch fabrication.

Phantom Skin Mimicking Gel Fabrication: 2% Agarose (Sigma Aldrich) was weighted in a 20mL Crystal Clear Borosilicate vial in DI water. Solution was heated a 175 C until solution turned transparent. Later, the temperature was lowered to 120C and casted onto 1.5mm, 3.0mm or 4.5mm Eco-Flex negative molds. Solution was let it dry for 2 min and further removed form mold with help of tweezers. Phantom skin mimicking gel were soaked in PBS pH 7.4 prior use.

Microneedle characterization. Bright field, fluorescent and merged images of the microneedles were obtained with an EVOS FL microscope coupled with 4 \times and 20 \times objectives with a fluorescence filter for a green and red-light excitation. The scanning electron

microscopy (SEM) images were captured with the use of a FEI Quanta 250 ESEM instrument (Hillsboro, Oregon, USA), using an acceleration voltage of 2-5 kV. The array was previously sputtered with an Iridium coating. The Energy-Dispersive X-Ray Spectroscopy (EDX) mapping analysis was carried out with an Oxford EDS detector attached to an SEM instrument and controlled by a Pathfinder software. Mg particles from microneedles were tested in the presence of tracer particles (0.9 μ m Nile red fluorescent particles from Sphero Tech) to study the mean square displacement of the activity of the Mg microparticles at different pH. Stack of images were analyzed by Image J Software, Flow trace plug in (1s particle trajectory image stacking).

Mechanical Testing: A mechanical test was performed to all microneedles by applying a constant load to a single tip. The mechanical strength of microneedles was measured by visualizing the displacement of the plate when intimate contact with the microneedle tip structure compared to the relative height of the cone. The fracture point was determined when a dramatic drop in force was experienced. The applied force was done with the use of a Force Gauge Model M4-20 system Mark0-10 Series 4.

In vitro Release Kinetics: Microneedles were subjected to a test of piercing and further dissolved into a 3mm thickness 2% Phantom Tissue Skin with a PBS pH 7.4 reservoir below. Both passive and active microneedles (n=5) were loaded with 50 μ g of Rhodamine 6G or IgG-HRP. After piercing for different set times, the supernatant was collected and analyzed by using a UV-2450 Shimadzu spectrophotometer from 300 to 700nm. For the electrochemical measurement of IgG-HRP, a reservoir with TMB+H₂O₂ was placed below the phantom tissue and repetitive runs of amperometry at a fixed potential of +0.1V for 50 s were employed to analyze the current change behavior of both microneedle controls.

Skin penetration and diffusion studies: A 1.5mm thickness porcine skin area of 2x2cm was pierced by microneedles for both diffusion and active control studies. The microneedle

patches were placed for different interval times, 5, 10, and 20 min and further cross sectioned for analysis at room temperature.

Cell line: The B16F10 cell line was acquired from American Type Culture Collection (ATCC). B16F10 cells were cultured in Dulbecco's Modified Eagle's Medium (DMEM, Life Technologies), supplemented with 10% (v/v) fetal bovine serum (FBS, Atlanta Biologicals) and 1% (v/v) penicillin-streptomycin (Life Technologies). Cells were maintained at 37°C, 5% CO₂. The cell cultures were maintained below a 50% confluence and early passage culture were utilized for the experiments.

In vivo efficacy study in mice: All experiments were conducted in accordance with UCSD's Institutional Animal Care and Use Committee (IACUC). 6- to 8-week-old female C57BL/6 mice (The Jackson Laboratory) were used. 25,000 B16F10 cells were suspended in 50 µL PBS and were injected intradermally into the right flank of C57BL/6 mice on day 0. PBS or anti-CTLA4 antibody (100 µg, Clone, 9H10, BioXcell) was administered into mice by intratumoral injection (30 µL) or by microneedle on day 10 and day 17. Tumor volumes were measured using a digital caliper. The tumor volume (mm³) was calculated as (long diameter short diameter²)/2. Animals were sacrificed when tumor volume reached 1500 mm³. For the blank active microneedle control, a single patch was administered on day 10.

Histology: Haematoxylin and eosin (H&E) staining of kidneys, livers, lungs, and spleens sections of the mice treated with active MN were evaluated at 60 days after tumor inoculation by histology analysis. Organs from PBS treated mice were evaluated when tumor volume reached 1500 mm³.

Stereolithography 3D printed Microneedle Devices: The prototyping of solid microneedles is currently supported by paid or free commercial software (SolidWorks, Fusion360). The 3D microneedle STL models were transferred to a slicing software (AnyCubic Photon slicer⁶⁴), which sliced the 3d model into thousands of micron layers in a

30M file, later connected to the printer via USB. The file was uploaded to an AnyCubic Photon UV LCD 3D printer for the prototyping and printing. Microneedles were fabricated within a 115 x 65mm build plate, by using exposure times of 8s and step size of 20 μ m. This instrument projected a 25W UV light source that sits inside a stainless-steel snoot, through a photocurable material (AnyCubic colored resin). The 3D printer has a 2K LCD masking screen, masking LCD provides very fine printing details down to few micrometers. After the fabrication, the build plate containing microneedle devices was gently removed from the printer, and microneedle devices were detached. Supports printed to build the microneedle devices were removed, microneedles were rinsed in IPA and placed under an ultrasonic bath for the removal excess of uncured material. Microneedle devices were subsequently placed in a UV nail machine to post cure for 30 min.

Supporting Figures

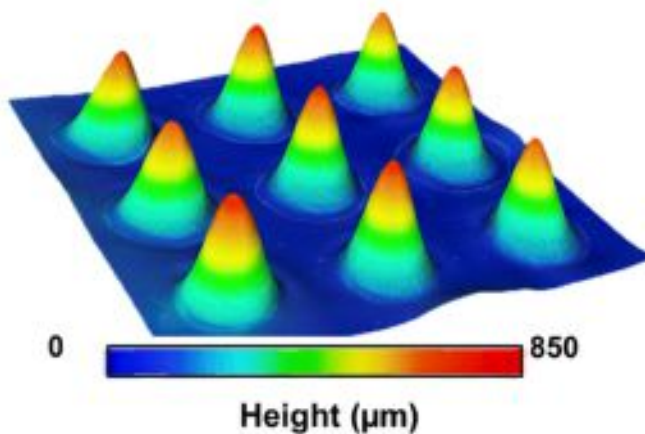


Figure s1. 3D height microscopy profile image of a 3x3 microneedle array.

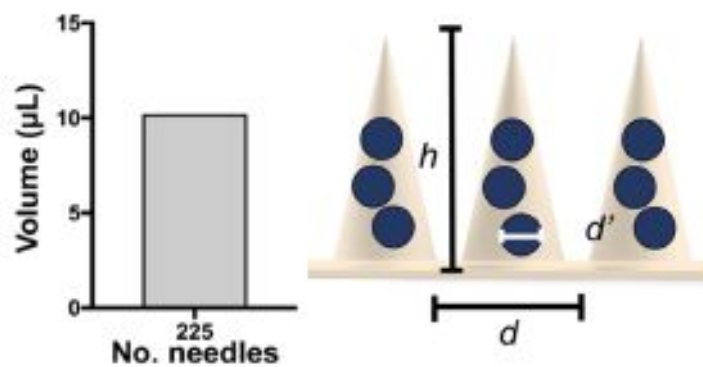


Figure s2. Theoretical loading of a characteristic MN patch containing 225 conical MN tips

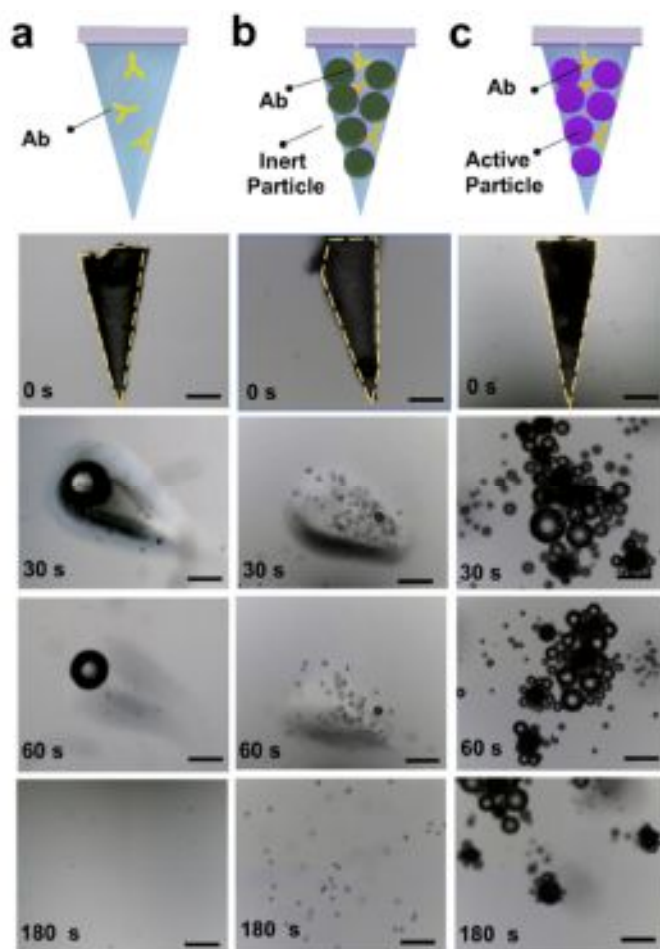


Figure s3. Schematic and time lapse images of the dissolution rate and fluid mixing of PVP microneedle under different experimental conditions: a) PVP Microneedle b) PS inert particle

PVP loaded microneedle and c) Mg PVP loaded active microneedle in PBS buffer pH 6. Scale bar, 200 μm

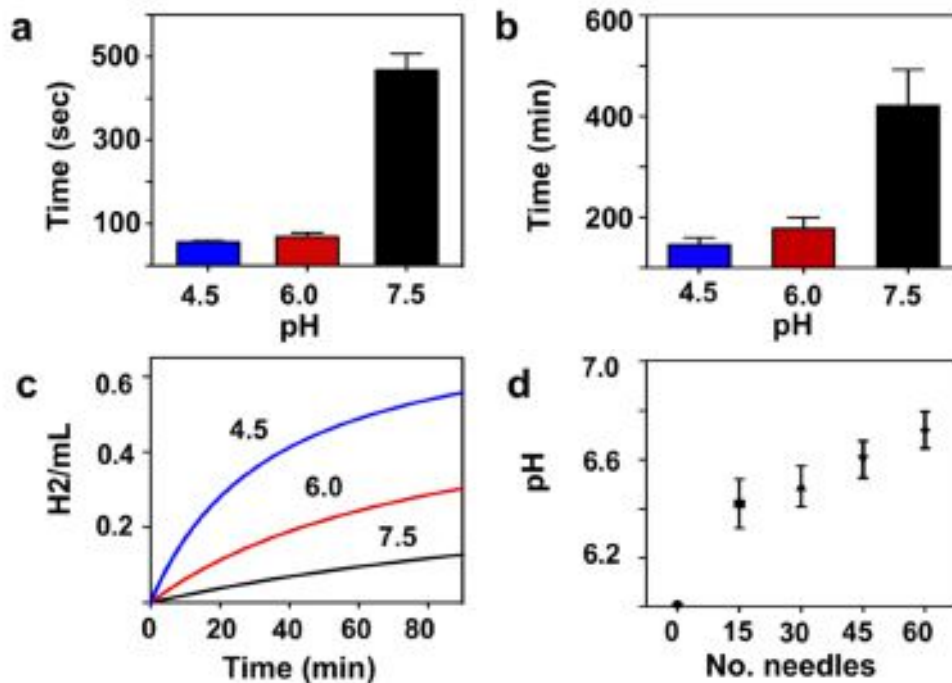


Figure s4. Active particle microneedle performance, activation and lifetime. a) Time necessary for Mg particles to start reacting ($n=5$). b) Degradation time of Mg particles ($n=5$). c) H₂ generation rate in the presence of different pH environments. d) pH solution variation of active needles after its complete dissolution (15 min).

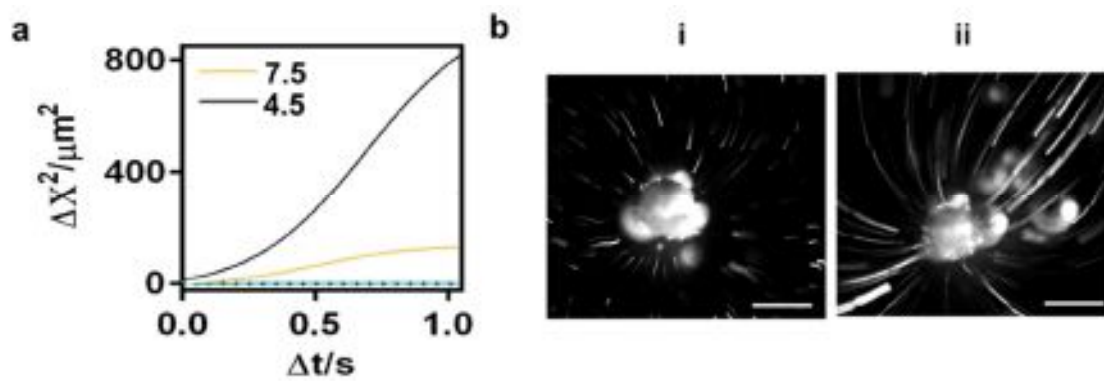


Figure s5. a) Mean Square Displacement of tracer particles in the presence of Mg particles at pH 4.5, and 7.5. b) Time-lapse images of the flow trace of 0.9 μm fluorescent beads used as tracer particles. i) pH 4.5, and ii) 7.5. Scale bar 100 μm .

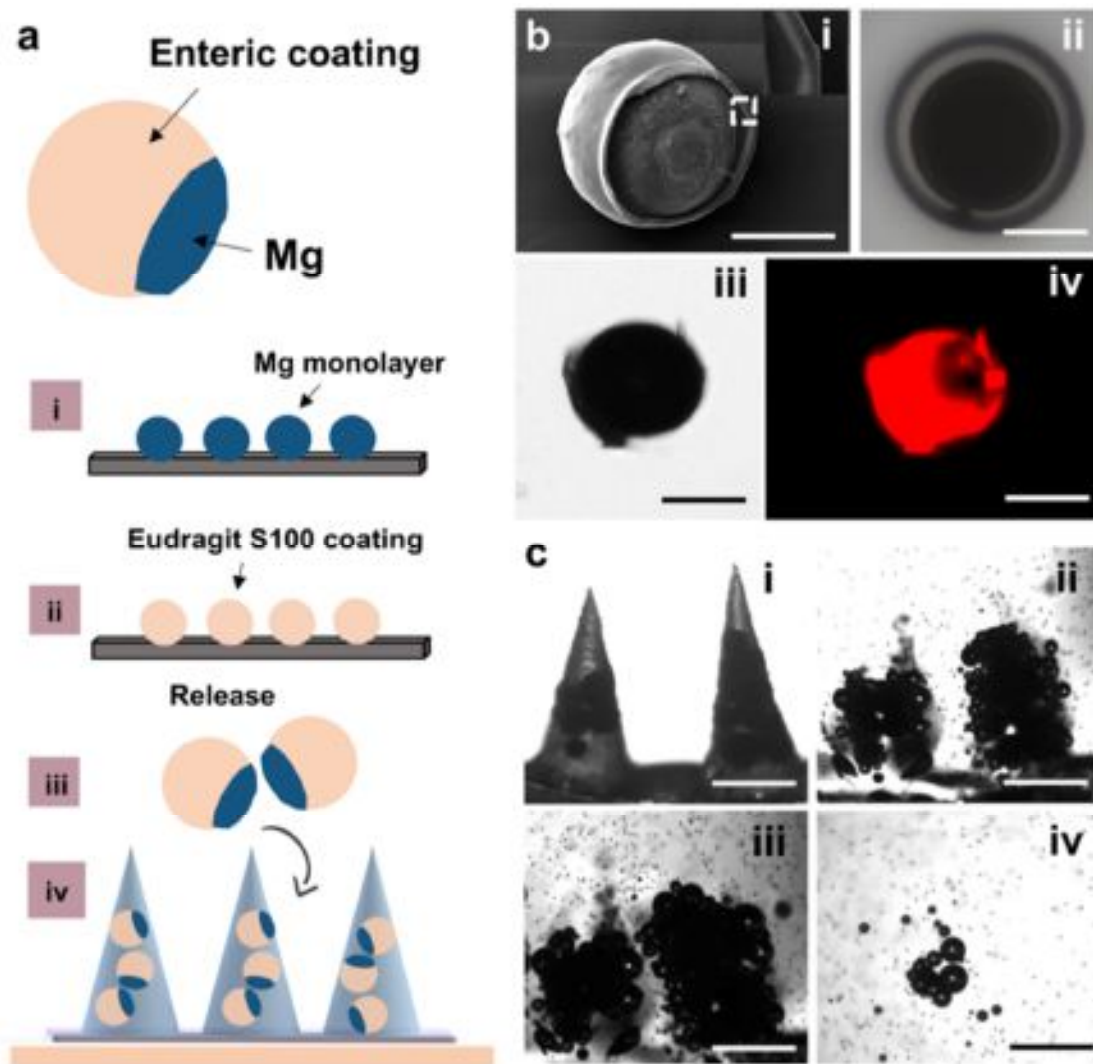


Figure s6. Tuning the capabilities of Mg particles to control a delayed activation. a) Enteric coating of an Eudragit S100 polymer (solubility $>\text{pH } 7.0$) made over mg particles. Mg monolayer (i), Eudragit s100 coating (ii), release (iii), and loading into MNs (iv). b) Scanning Electron Micrograph (i) optical microscopy image (ii and iii) and fluorescent image (iv) of Rh6G@Eudragit S100 coated mg particles. Scale bar, 50 μm . c) Time-lapse images of two

microneedle tips loaded with enteric coated Mg particles accelerating the dissolution of the transient polymer but with less reactivity compared to uncoated ones (i) before, (ii) 30 sec, (iii) 60 sec and (iv) at 180 sec. Coating provides directionality to the microparticles, thus reducing reactivity but extending degradation time (d). Scale bars, 400 μm .

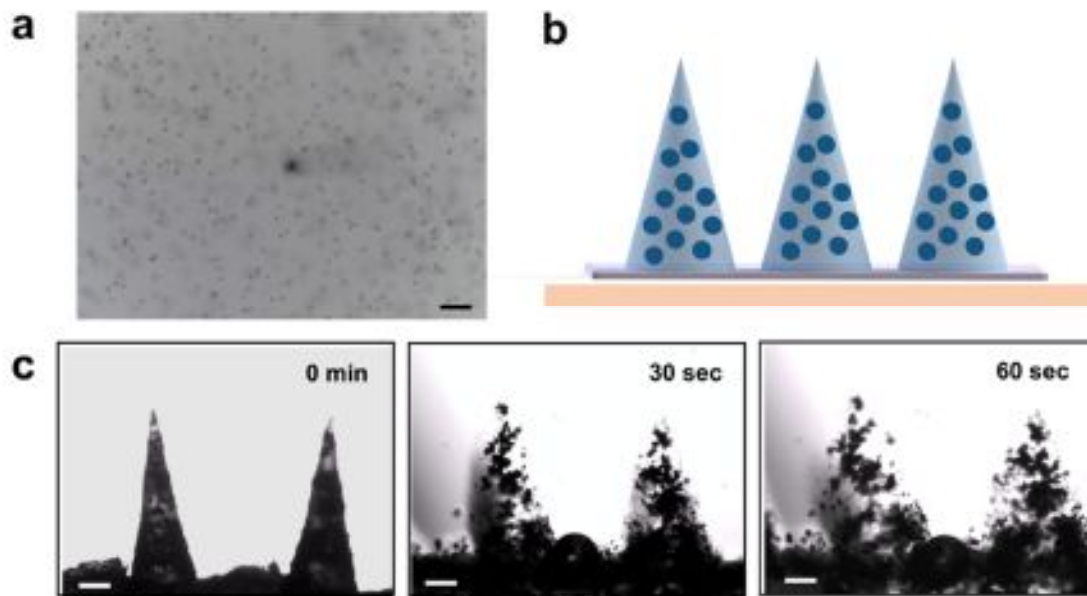


Figure s7. Microneedles loaded with 20 μm Mg particles. a) Flow trace of Mg particle with tracer 20 μm PS particles. Scale bar, 200 μm . b) Schematic of MNs loaded with 20 μm Mg particles. c) Time-lapse images of two microneedle tips loaded with 20 μm Mg at different time intervals: (a) 0 min, (b) 30 sec, (c) 60 sec. Scale bars, 200 μm .

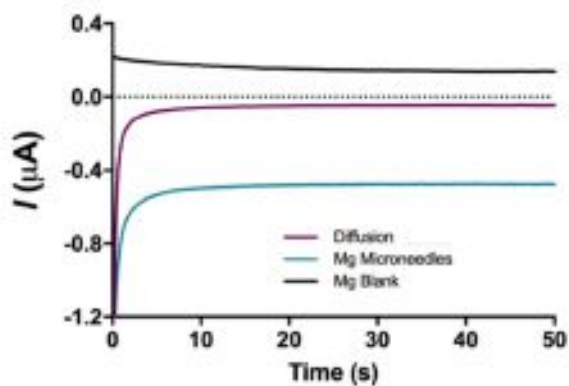


Figure s8. Amperometric curves of IgG-HRP from 3 release kinetics microneedle controls at the mark of 30 min (antibody that passed through the phantom tissue).

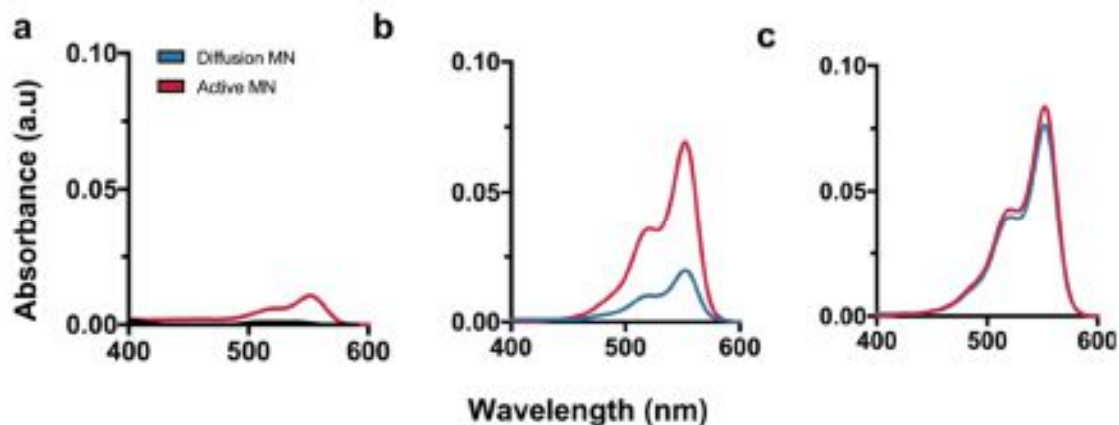


Figure s9. UV-vis spectrum of released Ab (IgG-AlexaFluor-555) from diffusion and active MNs at different time points, a) 10 min, b) 20 min, and c) 30 min. Ab content was measured from PBS buffer reservoir located below a 1.5 mm of thickness phantom tissue.

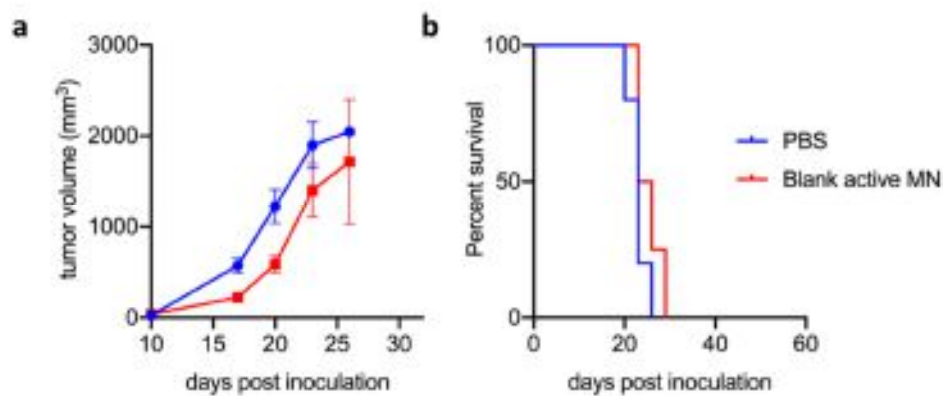


Figure s10. a) Tumor volumes growth curve of averaged tumor volumes of mice receiving PBS (blue, n=5), blank active microneedle (red, n=4). b) Survival rates of PBS and blank active microneedle treated groups.

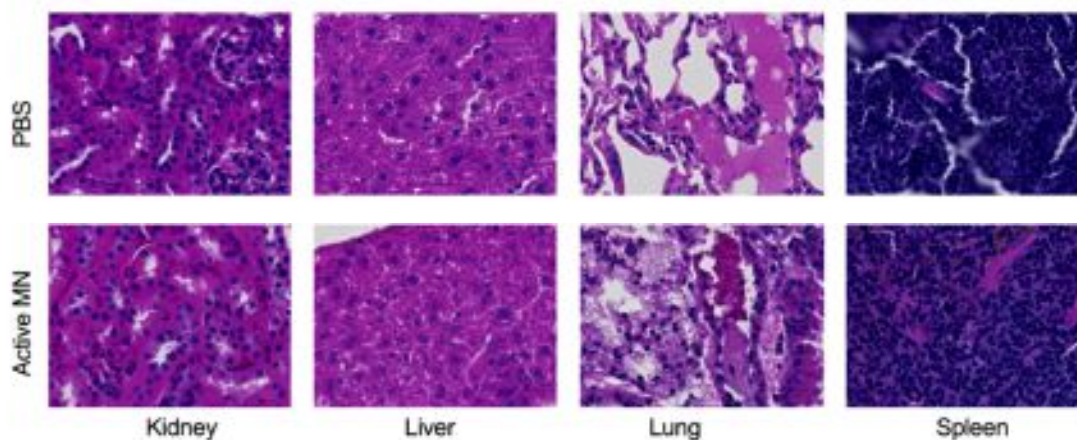


Figure s11. Histological assessment of the kidney, liver, lung, and spleen in PBS-treated and active MN treated mice.

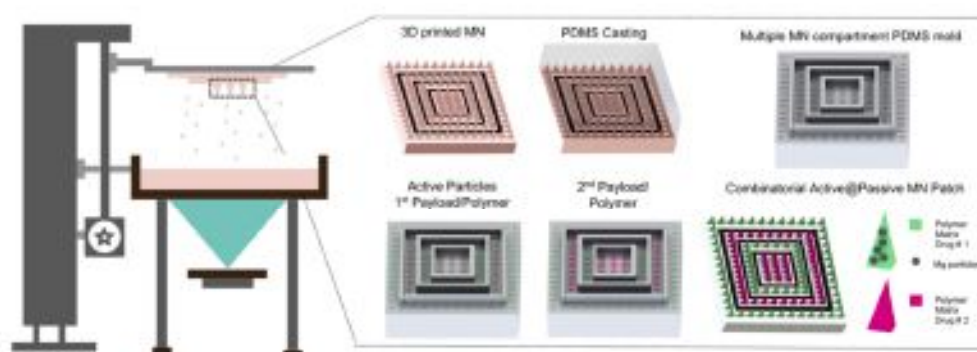


Figure s12. 3D printing and fabrication steps of polymeric combinatorial microneedle patch with spatially-resolved active and passive microneedle zones.